Available online at www.sciencedirect.com
ScienceDirect
Earth and Planetary Science Letters 260 (2007) 201–211
EPSL
www.elsevier.com/locate/epsl

A computational study of ionic vacancies and diffusion in $MgSiO_3$ perovskite and post-perovskite

Bijaya B. Karki [a,b,*], Gaurav Khanduja [a]

[a] Department of Computer Science, Louisiana State University, Baton Rouge, Louisiana 70803, USA
[b] Department of Geology and Geophysics, Louisiana State University, Baton Rouge, Louisiana 70803, USA

Received 14 February 2007; received in revised form 9 May 2007; accepted 19 May 2007
Available online 26 May 2007
Editor: G.D. Price

Abstract

We have performed first-principles simulations within density functional theory to investigate the effects of pressure on the formation of defects (ionic vacancies) and ionic diffusion in the perovskite (pv) and post-perovskite (ppv) phases of $MgSiO_3$. Our results show that the predicted formation enthalpies of three Schottky (MgO, SiO_2 and $MgSiO_3$) defects are similar between the two phases at high pressures (100 to 150 GPa) with MgO Schottky defect being the most favorable. However, the calculated activation enthalpies and activation volumes of diffusion are shown to differ substantially between them. In particular, the activation enthalpies for Mg and Si diffusion in ppv are smaller than the corresponding values for pv, for example, by factors of 2.2 and 3.4, respectively, at 120 GPa, whereas the O migration enthalpy of ppv is only slightly larger than that of pv. The easy migration paths of the cations in ppv are shown to take place along the ⟨100⟩ direction in which Si–O octahedra share the edges. Visualization of the simulation data reveals that the vacancy defects and migrating ions induce substantial distortions in the atomic and electronic structures around them. It is suggested that diffusion is equally easy for all three species in ppv and is likely to occur through extrinsic processes near the bottom of the lower mantle.
Published by Elsevier B.V.

Keywords: defects; diffusion; high pressure; $MgSiO_3$; first-principles simulation; scientific visualization

1. Introduction

Recent experimental and computational studies have shown that $MgSiO_3$ transforms from the perovskite (pv) phase to the post-perovskite (ppv) phase under lower mantle conditions (Murakami et al., 2004; Oganov and Ono, 2004; Tsuchiya et al., 2004a) suggesting that the D″ region consists primarily of the ppv phase. Possible implications of the transition and of the properties of the new phase for the deep lower mantle, particularly, for the D″ region are being studied extensively. For instance, the equations of state (Oganov and Ono, 2004; Tsuchiya et al., 2004a), elastic wave velocities and anisotropy (Tsuchiya et al., 2004b; Iitaka et al., 2004; Oganov et al., 2005; Wookey et al., 2005) and phonon spectra (Tsuchiya et al., 2005) of ppv have previously been calculated using the first-principles methods. The two phases of $MgSiO_3$ are found to have several interesting differences in their physical properties, which are used/expected to explain key seismic observations of the D″ region such as velocity

* Corresponding author. Department of Geology and Geophysics, Louisiana State University, Baton Rouge, Louisiana 70803, USA.
E-mail address: karki@csc.lsu.edu (B.B. Karki).

0012-821X/$ - see front matter. Published by Elsevier B.V.
doi:10.1016/j.epsl.2007.05.031

discontinuities, lateral heterogeneities and anisotropy (Murakami et al., 2004; Oganov and Ono, 2004; Iitaka et al., 2004; Tsuchiya et al., 2004a,b; Oganov et al., 2005; Wookey et al., 2005; Tsuchiya et al., 2005; Ono and Oganov, 2005; Wentzcovitch et al., 2006; Hirose, 2006), and also to model mantle electrical conductivity (Oganov et al., 2005; Ono et al., 2006).

Among several physical properties of the pv and ppv phases of $MgSiO_3$ that need to be better understood are rheological properties at high pressure. Knowledge about the defect energetics (formation and migration), and related atomic and electronic structures is critical to our understanding of mantle rheology because defects control diffusion and creep processes. For instance, the dominant diffusion mechanism may be vacancy-hopping and even the dominant deformation mechanism may be diffusion creep or diffusion-controlled dislocation climb. Ionic diffusion also determines electrical conductivity in minerals, which is important in modeling mantle conductivity (Hermance, 1995). In recent years, first principles studies of defective crystals have become common (e.g., Brodholt, 1997; Brodholt and Refson, 2000; Braithwaite et al., 2003; Carrasco et al., 2004; Alfe et al., 2005). To obtain reasonably accurate results for defects require quantum mechanical simulations of a relatively large atomic system. We have recently studied, from first principles, vacancy defects and migration in MgO (Karki and Khanduja, 2006a), and also studied vacancy defects in $MgSiO_3$ pv (Karki and Khanduja, 2006b) as a function of pressure. To the best of our knowledge, only simplified model calculations of defects and diffusion in pv were previously performed (Wall and Price, 1989; Wright and Price, 1993; Watson et al., 2000). Also, a relatively few experimental studies of ionic diffusion in pv at high pressures currently exist (e.g., Yamazaki et al., 2000; Dobson, 2003; Holzapfel et al., 2005).

In this paper, we report important results on the energetics, geometry, and electronic structure of defects and diffusion in the pv and ppv phases of $MgSiO_3$ at geophysically relevant pressures using the first-principles computational method based on density functional theory. The defects studied are ionic vacancies with charge states of 2+, 4+ and 2−, respectively, on cationic (Mg and Si) and anionic (O) sublattices, which allow us to study Schottky defects of different types as in the previous studies (Wall and Price, 1989; De Vita et al., 1992; Wright and Price, 1993; Watson et al., 2000; Walker et al., 2003; Alfe et al., 2005; Karki and Khanduja, 2006a,b). Our focus is on defect migration (diffusion) in pv and on both defect formation and migration in ppv to understand how defects and diffusion compare between the two phases at deep mantle pressures.

2. Methodology

Calculations are performed using the parallel code PWscf (Plane-Wave Self-Consistent Field), which is an implementation of density functional theory within the local density approximation (Baroni et al., 1987; Giannozzi et al., 1991). A plane wave basis set with cutoff of 70 Ry is used to expand the valence electronic wave function and Brillouin Zone summations of electronic quantities are performed on $2\times2\times2$ k-mesh (Monkhorst and Pack, 1976). Other computational details can be found elsewhere (Karki and Khanduja, 2006a,b). Supercells containing 80 and 60 atoms are used, respectively, for $MgSiO_3$ pv and ppv. They are large enough to get fully converged results, as also tested previously (Karki and Khanduja, 2006b). The defective cell contains only one charged defect of given type at a time. Two types of cation vacancy are created; one by removing an Mg core leaving two valence electrons in the system and other by removing an Si core leaving 4 electrons in the system. An anion vacancy is formed by removing an O core together with eight valence electrons. There are two distinct O sites in the orthorhombic structure; however, their vacancy formation energies are within 1% for both pv and ppv so we consider only one O vacancy without making a distinction between them. Thus, the net charges of the Mg, Si and O vacancies are −2e, −4e and 2e, respectively. These ionic vacancies form the Schottky defects — the dominant point defects. Such defects were previously studied in silicate phases (Wall and Price, 1989; Wright and Price, 1993; Watson et al., 2000, 2003; Karki and Khanduja, 2006b). Other charge states including F center (neutral O vacancy) are also possible; however, they are not of interest here.

Due to a net defect charge (q) associated with the supercell used, two treatments are needed to obtain acceptable results. The first is to use the Ewald sum for the long-range columbic interactions by assuming that there is a counter-charge, which is distributed uniformly throughout the simulation cell (Leslie and Gillan, 1985). The second is to make appropriate correction for defect–defect interactions arising from a periodic array of defective cell because we are interested in the energy of an infinite lattice containing only one defect. The defect–defect correction (Leslie and Gillan, 1985; Brodholt, 1997; Lento et al., 2002) is given by $\Delta E=-\alpha^* q^2/\varepsilon$. The value of α^* varies from 2.266 at zero pressure (the largest supercell) to 2.513 at 150 GPa (the smallest

supercell) for the 80-atom pv system. It varies from 2.774 and 2.845 between 100 and 150 GPa for the 60-atom ppv system. The values of dielectric constant (ε) used are the same as those used in our previous studies (Karki and Khanduja, 2006b).

We use a constant-volume approach in which cell parameters are not allowed to relax in a defective system. We have shown that the constant-volume approach used here and the other constant-pressure approach, e.g. (Watson et al., 2000) essentially produce very similar results as long as the defect related enthalpy is concerned (Karki and Khanduja, 2006b). Atomic positions are fully optimized in the supercell containing a single defect of a given type. The fully relaxed energies of the perfect and defective supercells are used to determine the vacancy extraction and Schottky defect enthalpies. To calculate the migration enthalpy of a given type of vacancy, we remove the corresponding ion from two nearest neighboring sites and then constrain one of the removed ions to lie halfway between the sites. One can view this as a vacancy hopping process in which an ion leaves its current site and heads towards other vacancy site by crossing the maximum barrier height at the saddle point. The resulting energy when the migrating ion is positioned at the middle of the line joining two neighboring half-vacancies is then subtracted from the energy of the corresponding equilibrium vacancy system. The migration enthalpies are not affected by defect-defect correction since the same correction applies to both equilibrium and migrating vacancy systems. We perform simulations for pv and ppv over the pressure regimes of 0 to 150 GPa, and 100 to 150 GPa, respectively.

3. Results and discussion

3.1. Defect energetics

For the both pv and ppv phases of $MgSiO_3$, we calculate the fully relaxed energy of the supercell with no defect and that of the supercell containing single charged defect of each type. Three point defects studied include two cationic (Mg^{2+} and Si^{4+}) vacancies and one anionic (O^{2-}) vacancy. The defect extraction energy can be obtained by subtracting the energy of the defective crystal from that of the perfect crystal and then subtracting the correction (ΔE) for the defect–defect interaction:

$$E_{\mathrm{ION}}(V) = E(N-1,V) - E(N,V) - \Delta E \qquad (1)$$

Here, $E(N,V)$ is the energy of the perfect crystal containing N lattice sites at a given pressure P whereas $E(N-1,V)$ refers to the energy of system, which contains an isolated vacancy defect (i.e., either Mg or Si or O ion missing). Note that the energy difference between the perfect and defective crystals as defined here is not equal to the vacancy formation enthalpy. One must take into account the energy of the isolated ion at infinity, which can be computed by placing the corresponding ion in a large cubic box, e.g. (Carrasco et al., 2006), however, this appears to make sense only in the case of zero pressure.

The individual vacancy formation enthalpies are not of major concern because ions are not removed to infinity but rather removed to create a formula unit of the same or another phase. In other words, our interest is to compute the Schottky defect formation enthalpy, which is needed to remove one formula unit of $MgSiO_3$ or MgO or SiO_2 and add to it to the surface (Wall and Price, 1989; Wright and Price, 1993; Brodholt, 1997; Watson et al., 2000; Alfe et al., 2005; Karki and Khanduja, 2006a,b). The full Schottky defect enthalpy (H_S), which is simply the sum of extraction energies of one Mg^{2+}, one Si^{4+} and three O^{2-} vacancies minus the energy per formula unit, is then calculated (Table 1) using

$$H_S = E_{\mathrm{Mg}}(V) + E_{\mathrm{Si}}(V) + 3E_{\mathrm{O}}(V) + H_{\mathrm{MgSiO_3}} \qquad (2)$$

Note that $H_{\mathrm{MgSiO_3}}$ is the enthalpy of the removed formula unit, which also includes the PV term so the result is the Schottky formation enthalpy. Similarly,

Table 1
Calculated defect energetics (in the units of eV) of perovskite (pv) and post-pervoskite (ppv) for the relaxed structures and with corrections for defect–defect interactions included are shown

	pv, 0 GPa	pv, 120 GPa	ppv, 120 GPa
H_{Formula}	−1465.52	−1439.56	−1439.68
E_{Mg}: Relaxed	54.25	60.41	60.79
Corrected	55.58	61.65	62.20
E_{Si}: Relaxed	170.61	190.79	190.96
Corrected	175.94	195.75	195.59
E_{O}: Relaxed	416.95	407.95	407.59
Corrected	418.28	409.19	409.01
H_S: Relaxed	10.19	35.50	34.83
Corrected	20.85	45.42	46.09
Mg-Migration	3.47, ⟨110⟩	7.71, ⟨110⟩	3.49, ⟨100⟩
	13.54, ⟨001⟩	21.76, ⟨001⟩	8.36, ⟨101⟩
Si-Migration	8.33, ⟨110⟩	10.48, ⟨110⟩	3.05, ⟨100⟩
	19.56, ⟨001⟩	26.19, ⟨001⟩	6.82, ⟨001⟩
O-Migration	0.57, ⟨100⟩	2.57, ⟨100⟩	2.97, ⟨110⟩
	2.78, ⟨110⟩	4.85, ⟨110⟩	4.71, ⟨100⟩

H_{Formula} is the enthalpy per unit formula. E_{Mg} E_{Si} and E_{O} are Mg, Si and O extraction energies (see the text for the definition), respectively. Also shown are the migration energies for three types of ions for two directions in each case.

we also calculate the partial (pseudo) MgO and SiO_2 Schottky defect enthapies by using the enthalpies of MgO and SiO_2 formula units calculated for their rock-salt and stishovite phases, respectively.

Ionic diffusion mediated by vacancy hopping can be viewed as an ion moving from one site to a vacant site thereby crossing over the highest point or saddle point of the potential energy barrier. The enthalpy of vacancy migration is then given by the difference between the enthalpy of the interstitial at the saddle point (SP) and that of the ground state (GS)

$$H_M = H_{SP} - H_{GS} \quad (3)$$

This represents the activation enthalpy for diffusion in the extrinsic regime, where the vacancy concentration is a function of impurity content and thus is independent of temperature. However, the concentration depends on temperature in the intrinsic regime so one needs to add the defect formation enthalpy. Thus, the activation enthalpy for intrinsic diffusion (H_D) can be written as

$$H_D = H_M + H_S/n \quad (4)$$

where n is the number of ions in the Schottky defect, which is 5 for $MgSiO_3$, that is, one needs to add one fifth of the full Schottky enthalpy to obtain activation enthalpy for intrinsic diffusion.

The effects of ionic relaxation and system size are also explored. All free positional parameters are fully relaxed and the relaxation energies are shown to be substantial as in our previous studies (Karki and Khanduja, 2006a,b). The defect–defect corrections are included; and the corrected energies are shown to indeed converge very well for the system sizes considered here. Results are reported for the 80- and 60-site systems, respectively, for the pv and ppv phases. The calculated extraction energies and the effects of pressure on the defect formation enthalpies are very similar between the two phases (Table 1 and Fig. 1). The full Schottky formation enthalpy (H_S) increases by 7.93 and 7.09 eV for pv and ppv, respectively, over the pressure regime between 100 and 150 GPa. We also calculate two pseudo-Schottky defects formed by removing charge neutral units of MgO and SiO_2. At all pressures, the most stable defect is MgO pseudo-Schottky because its formation enthalpy is systematically lower than the both SiO_2 pseudo-Schottky and $MgSiO_3$ full Schottky enthalpies. For example, at 120 GPa, the enthalpies per atom for MgO and SiO_2 pseudo-Schottky defects are 7.58 and 11.04 eV, respectively, for ppv, which are slightly larger than the corresponding values of 7.46 and 10.99 eV for pv. Note that the full Schottky enthalpy per atom is 9.22 eV for ppv and 9.08 eV for pv at 120 GPa. Our results at high pressure compare favorably with previous model calculations (Wright and Price, 1993, Watson et al., 2000).

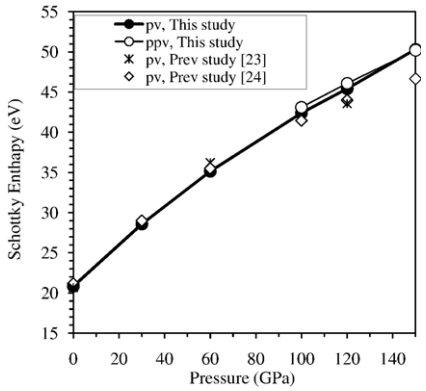

Fig. 1. Pressure dependence of the Schottky formation enthalpy of perovskite (filled circles) and post-perovskite (open circles). Also shown are the results from previous calculations for perovskite: asterisks (Wright and Price, 1993) and diamonds (Watson et al., 2000). The errors are within the size of the symbols used.

To calculate the migration enthalpy, we choose the saddle point at which a migrating ion is placed to be situated exactly halfway between the initial and destination sites from where the ions are removed to create vacancy sites. For each species, two different migration directions are considered (Table 1). The initial and destination sites when they are closest to each other are found to give the minimum migration energy in most cases. This is consistent with previous MD study of pv (Wright and Price, 1993), which showed that the saddle point lies approximately halfway between the two closest (initial and destination) sites by placing a migrating ion at various points between the two sites. We first discuss diffusion in pv at zero pressure. Mg diffusion is shown to take along the ⟨110⟩ axis. The saddle point situated at halfway between the two sites along this direction gives activation enthalpies for migration of 3.47 and 7.62 eV for extrinsic and intrinsic diffusion, respectively. For Si diffusion, we find the ⟨110⟩ direction as the most likely path for which the calculated enthalpies are 8.33 eV in extrinsic regime and 12.48 eV in intrinsic regime. For O ion, diffusion in the ⟨100⟩ direction is predicted to be the most favorable, with activation enthalpies of 0.57 and 4.72 eV, respectively, for extrinsic and intrinsic diffusion. With increasing pressure, the diffusion pathways remain unchanged but the activation enthalpies increase monotonically (Fig. 2). The activation enthalpies of the cations are found to be considerably higher than the corresponding

values for the anion at all pressures. Our results at zero and high pressures are comparable with those from a previous MD study (Wright and Price, 1993), which sampled migration pathway at several interstitial positions.

To compare with the experimental data for the activation enthalpies of diffusion (extrinsic) in $MgSiO_3$ pv, which were measured at temperatures of 1500–2000 K and pressures of 22 to 26 GPa, we use our results for extrinsic diffusion at 30 GPa. For O diffusion, the calculated value of 1.41 eV is almost equal to the measured value of ~1.4 eV at 24 GPa derived from electrical conductivity experiments (Dobson, 2003). Our result of 4.78 eV for Mg diffusion correlates well with the reported activation enthalpy of 4.29 eV for Fe–Mg interdiffusion (Holzapfel et al., 2005). Unlike the case of O and Mg diffusion, the calculated activation enthalpy for Si diffusion of 9.10 eV is much higher than the corresponding experimental value of 3.48 eV (Yamazaki et al., 2000). One possible explanation for such a large discrepancy could be that Si diffusion in a real sample can be easier in the presence of O vacancies. Previous calculations (Karki and Khanduja, 2006b) have shown that the presence of an O vacancy lowered the activation enthalpy of extrinsic Si diffusion from 9.20 to 7.64 eV at zero pressure, and 10.32 to 4.79 eV at 125 GPa. We also find a similar trend: In the presence of an O vacancy, the extrinsic activation enthalpy decreases from 8.33 to 6.84 eV at 0 GPa, 9.10 to 6.81 eV at 30 GPa, and 10.48 to 5.62 eV at 120 GPa. The new value of 6.81 eV is still much larger than the experimental value. This discrepancy between the computational and experimental results requires more work.

We now discuss diffusion of ppv and compared it with that of pv at high pressure. Our results show that vacancy migration differs substantially between pv and ppv (Fig. 2). First, the activation enthalpies for diffusion of all three ions for ppv are similar to each other. Second, the Mg and Si enthalpies of ppv are much lower than those of pv whereas the O migration enthalpy of ppv is slightly higher than that of pv. At 120 GPa, the activation enthalpies of extrinsic and intrinsic diffusion in pv are, respectively, 7.71 and 16.79 eV for Mg, 10.48 and 19.56 eV for Si, and 2.57 and 11.65 eV for O. However, these values for Si in the presence of an O vacancy are 5.62 and 23.78 eV. The Mg and Si values are so high that their bulk diffusion in the pv phase would be difficult both in intrinsic and extrinsic regimes at the deep mantle conditions. On the other hand, the corresponding values of extrinsic and intrinsic diffusion in ppv are, respectively, 3.49 and 12.71 eV for Mg, 3.05 and 12.27 eV for Si, and 2.97 and 12.19 eV for O atoms. Third, the directions of ⟨100⟩, ⟨100⟩ and ⟨110⟩, respectively, for energetically most favorable Mg, Si and O migration paths in ppv differ from the corresponding migration directions in pv. Thus, the activation enthalpies as well as the migration directions change across the pv-to-ppv phase transition.

We also calculate the activation volumes defined as

$$V_M = \frac{dH_M}{dP} \text{ and } V_D = \frac{dH_P}{dP} \quad (5)$$

respectively, for diffusion in the extrinsic and intrinsic regimes. Our results for activation volumes for extrinsic

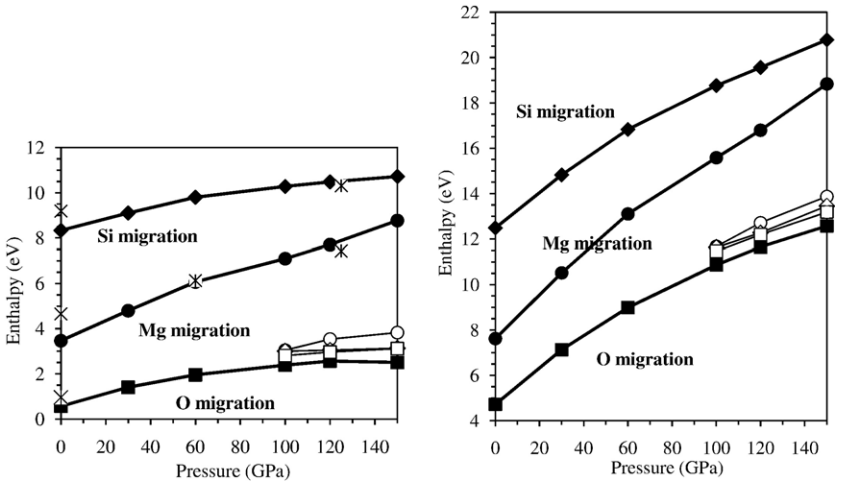

Fig. 2. Pressure dependence of the activation enthalpies for extrinsic (left) and intrinsic (right) diffusion in perovskite (filled symbols) and post-perovskite (open symbols). The circles, diamonds and squares represent the Mg, Si and O migration enthalpies, respectively. Also shown are the results from previous calculations for perovskite: asterisks (Wright and Price, 1993). The errors are within the size of the symbols used.

Table 2
Calculated activation volumes (in the units of cm^3/mol) for extrinsic (V_M) and intrinsic (V_D) diffusion in perovskite (pv) and post-pervoskite (ppv)

		pv, 0 GPa	pv, 120 GPa	ppv, 120 GPa
Mg:	V_M	4.28	3.17	1.61
	V_D	9.33	6.20	4.38
Si:	V_M	2.48	0.87	0.25
	V_D	7.53	5.18	3.44
O:	V_M	2.71	0.34	0.61
	V_D	7.75	3.36	3.85

and intrinsic diffusion of all three species for pv and ppv are shown in Table 2. The values of V_D are systematically larger than those of V_M for each phase since H_D increases more rapidly with pressure than H_M. Like the activation enthalpies, the activation volumes of diffusion also show large differences between the two phases of $MgSiO_3$. The values of V_M and V_D of ppv are smaller than those of pv for diffusion of Mg and Si, however, the opposite is true for O diffusion. Again, our results for pv are comparable with previous results (Karki and Khanduja, 2006b). The value of V_M for Mg diffusion at 120 GPa from this study is 1.61 cm^3/mol, compared to a previous value of 2.10 cm^3/mol obtained for the range of 0 to 125 GPa. Similarly, the present result of V_M for Si diffusion at 120 GPa is 0.87 cm^3/mol, compared to a previous value of 0.86 cm^3/mol. However, in the presence of an O vacancy, our predicted v_M is negative (−1.24 cm^3/mol), consistent with the previous result of −2.2 cm^3/mol. There are no experimental data for $MgSiO_3$ but the experimental values for MgO at 25 GPa (Van Orman et al., 2003) are 3.0 and 3.3 cm^3/mol, respectively, for extrinsic Mg and O diffusion.

3.2. Atomic structure

Visualization of simulation data allows us to analyze the distortion of atomic configuration induced by a given point defect (Bhattarai and Karki, 2006). The vector data used for visualization are the displacements of individual atoms in a defect crystal relative to their positions in a perfect crystal. Each atom is displayed as a sphere whose size is proportional to the magnitude of the displacement. The orientation of the line starting from the surface of the sphere represents the direction of the displacement. Visualization of the fully relaxed vacancy systems reveals that relaxations of atoms of different types at different distances from the defect site differ in the magnitude as well in the direction (Fig. 3). The spheres close to the defect site are relatively large implying that the most relaxation occurs in the immediate vicinity of the defect site. We have previously presented a detailed analysis of the atomic distortion induced by Mg-, Si- and O- site vacancies in the pv phase for the supercell consisting of 160 atoms (Karki and Khanduja, 2006b). Here, we briefly present the structural results in the case of 80-site supercell at 120 GPa, which agree favorably with our previous prediction. In the case of the negatively charged Mg-site vacancy (V_{Mg}), the neighboring O ions (red spheres), which define the eight-fold Mg–O coordination in a perfect crystal, are pushed away from the defect site. The distances between the vacant site and adjacent O atoms denoted by the V_{Mg}–O distances, increase by 2 to 4.5% of the Mg–O bond lengths of perfect crystal. For the negatively charged Si-site vacancy (V_{Si}), all six O atoms, which are coordinated to the vacant site, are displaced away from the vacancy site. As a result, the V_{Si}–O distances increase by 0 to 4.5 %. Four Mg have moved towards the defect site by the largest amount and other four Mg atoms have also moved towards the site so that the vacant site-Mg distances decrease by 3.6 to 10.5%. For the positively charged O-site vacancy (V_O), the two Si atoms, whose octahedra share the O vacancy site as one of their six vertices, see the maximum outward displacement. The V_O–Si distances increase by 9.5%.

Our structural analysis suggests that ppv (Fig. 3) shows a qualitatively similar defect-induced atomic distortion as in pv. Also note that the defect formation enthalpies are very similar between these phases. In ppv, the Mg-site vacancy pulls inward the neighboring O ions (red spheres), which define the eight-fold Mg–O coordination in a perfect crystal, much less than it pushes away Si and Mg atoms. The V_{Mg}–O distances increase by 0.5 to 1.1%. Two Si atoms (blue spheres) lying on the *bc*-plane see inward movements much more than four Si atoms lying on the *ca*-plane. The corresponding distances decrease by 3.7 and 1.6%. Only two Mg atoms (green spheres) are pulled towards the defect site with the V_{Mg}–Mg distances decreased by 3.9%. For the Si-site vacancy, all six O atoms, which are coordinated to the vacant site, are displaced away from the vacancy site. The V_{Si}–O distances increase by 5.5% for two apical O (corner sharing vertices) and 7.3% for basal O (edge sharing vertices). Two Mg have moved towards the defect site by the largest amount, compared to other four Mg atoms so that the corresponding vacant site-Mg distances decrease by 12.1 and 4.8%. Also two Si atoms see large inward motion along *a*-direction with V_{Si}–Si distances decreased by 4.2%. Finally, for the O-site vacancy, the two Si atoms, whose octahedra

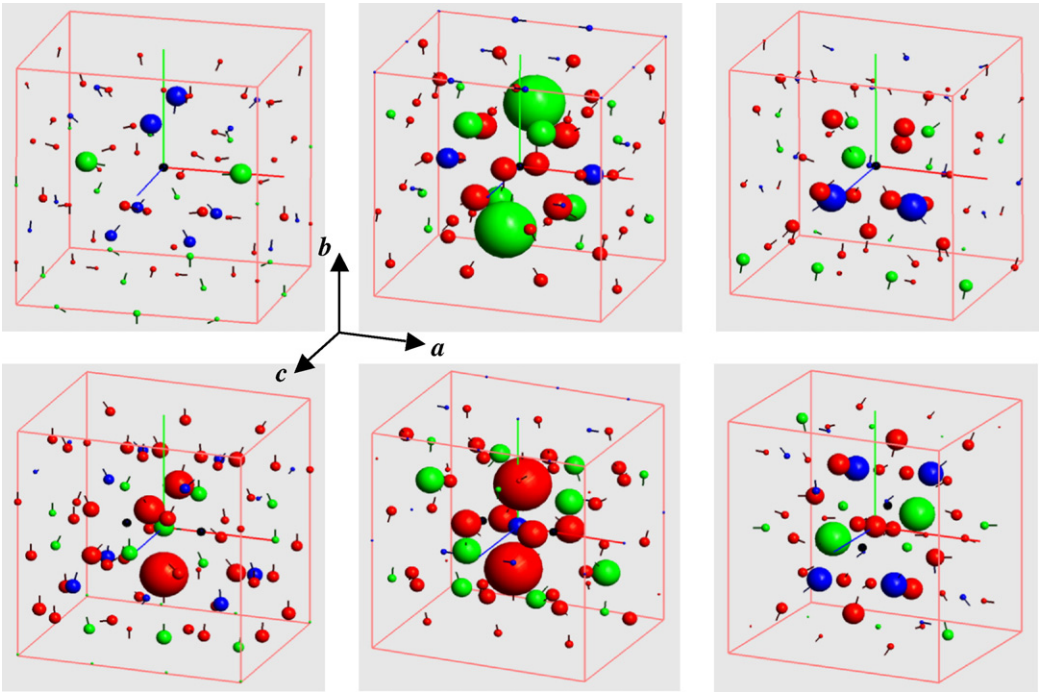

Fig. 3. Visualization of atomic displacements. Upper row: Mg (left), Si (center), and O (right) vacancies in the 60-site post-perovskite system at 120 GPa. Green, blue and red spheres represent Mg, Si and O atoms, respectively. A black sphere at the center of the supercell indicates the defect (vacant site) site. Lower row: Mg (left), Si (center) and O (right) migrating ions located at the center of the supercell. Adjacent vacancy sites are indicated by two black spheres located on each side of the center along the line of migration.

share the O vacancy site as one of their six vertices, see the maximum outward displacement with the V_O–Si distances increased by 6.5%. Ten O atoms move away from the defect site and the V_O–Si distances decrease by 1.1 to 3.7%. Mg atoms are also pushed away from the defect site with V_O–Mg distances increased by 0.5 to 2.4%.

Easier diffusion of Mg and Si in ppv compared to that in pv can be attributed to structural differences between the two phases (Murakami et al., 2004; Oganov and Ono, 2004; Tsuchiya et al., 2004a). The ppv phase shows the layered structure consisting of alternate layers of Si-octahedra and Mg atoms, which are perpendicular to the ⟨010⟩ direction (Fig. 4). The octahedra share their edges along the ⟨100⟩ direction and remain connected at the apices along the ⟨010⟩ direction. The jump distances within the layer are shorter than those between the layers thereby making cationic diffusion within the corresponding layers easier than that in the direction perpendicular to the layer. Thus, in ppv, both Mg and Si diffusion are most likely to occur along the ⟨100⟩ direction. Visualization of the atomic displacement data (Fig. 3) suggests that migrating cations open their migration path along the ⟨100⟩ direction by pushing the nearest O atoms away from their positions: The migrating Mg ion pushes away three O atoms (roughly lying in the same plane parallel to the *bc*-plane) whereas the migrating Si atom pushes away two O atoms (apical). Unlike cations, the most likely O diffusion in ppv occurs between two octahedral layers instead along the octahedral edges.

3.3. Electronic structure

Charges associated with the cationic (Mg and Si) and anionic (O) vacancy defects are of opposite sign. They are expected to induce a strong distortion of the valence electron clouds on neighboring ions. In the case of vacancy migration, the distortion comes from two vacancies (corresponding to initial and destination sites) and one migrating ion placed between them. The electronic structures are explored in details by using the multiple datasets visualization method (Khanduja and Karki, 2006), which allows us to render more than one volume datasets simultaneously. To understand the electronic contributions arising only from defects, we visualize the electron density differences taken between defective and perfect systems (Fig. 5). Looking at such difference makes sense for the unrelaxed systems, i.e., before any ionic relaxation in the supercell with defect.

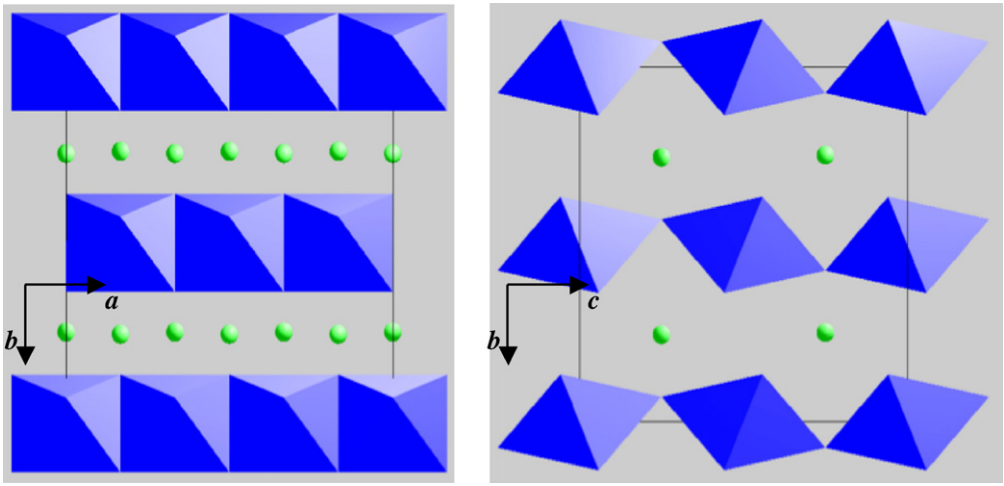

Fig. 4. Post-perovskite structure, view down the *c*-axis and *a*-axis. Si–O octahedral (blue) and Mg atoms (green spheres) are shown.

However, in the relaxed vacancy system, the charge distribution is also influenced by atomic displacements. So we place back the missing ion(s) at the corresponding vacancy site(s) (and remove the migrating ion) in the fully relaxed defective system, and take the difference between this new system and the original relaxed defective system. The defect-induced electronic structures thus extracted before and after structural relaxations are found to be very similar. So we only present the visualization of the charge density differences

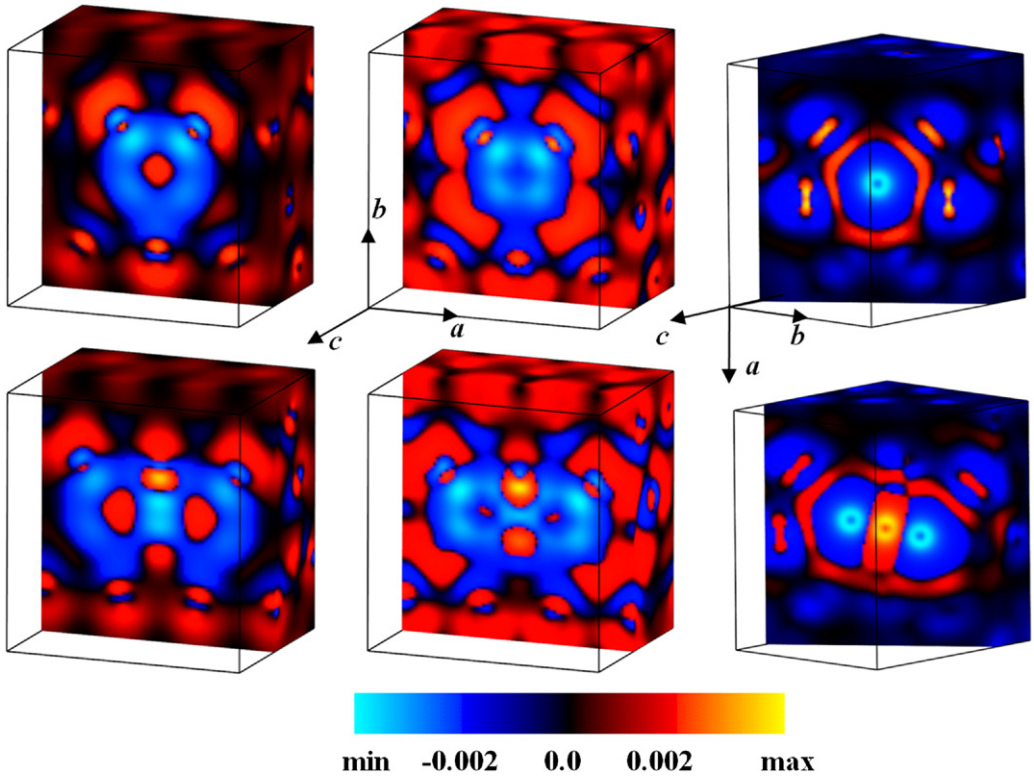

Fig. 5. Visualization of electron density difference (in units of $Å^{-3}$) in $MgSiO_3$ post-perovskite. Upper three images are for vacancies and lower three images are for migrating ions: Mg (left), Si (center) and O (right). In each case, the vertical surface represents the clipping plane passing through the defect site or migrating ion site, which is located at the center of the image. Note that the plane also contains the migration direction.

(defective–perfect) taken for the unrelaxed systems. A clipping method is used to show the interior of the volume data. In each image, visible surfaces represent the planes passing through the defect site and/or the migration direction. A multiscale RGB (red, green, blue) color map is used in order to highlight the small-scale variations while keeping the overall context on the display. The black-to-red-to-yellow range maps the regions where electrons are deposited (moved in) and the black-to-blue-to-cyan range maps the regions where electrons are depleted (moved away).

Since valence electrons from Mg and Si atoms along with those from O atoms are primarily localized in the vicinity of O ions, defect-induced distortions are mostly manifested around O atoms for both vacancy and migrating ion. The defect-induced structures show similar pattern between the two phases so our discussion is only based on the electronic structure of ppv, shown in Fig. 5. Also, the effects of pressure are not substantial although the sizes and intensities of red and blue regions vary to some extent. The negatively charged Mg vacancy appears as the mostly blue region with small red at the center as the electrons are depleted away from this region. Also, the valence electrons on neighboring O ions are repelled by the negatively charged defect as displayed by blue regions surrounding the O sites and red regions towards Mg sites. Nearly the same behavior (with much smaller degree of distortion) is seen around the O sites further away from the defect. Also note that the mostly blue regions surrounding the defect site indicate depletion of electrons. The electronic structure around the Si vacancy is similar to that of the Mg vacancy. The positively charged O vacancy site appears as the blue (and cyan) region at the center of the image since the electrons are removed from this region along with the missing O atom. The electrons from the neighboring O ions are pulled towards the defect site as seen in the mostly red regions surrounding the defect site. The oxygen p orbitals pointing towards the vacancy are directly involved in the charge redistribution in all three cases; the effects are reflected in blue regions, which are mostly aligned towards the defect site. In the case of migrating ions, the electronic structures of the neighboring ions remain essentially unchanged, compared to those for non-migrating defects. The structures in the vicinity of each migrating ion clearly represent the existence of two half-vacancies separated by the ion itself.

4. Implications and conclusions

Knowledge about defects and diffusion in major mantle minerals plays an important role in modeling rheological properties of the Earth's mantle as the dominant deformation mechanism in the deep interior is thought to be diffusive in nature. We have calculated vacancy extraction and migration enthalpies as a function of pressure from 0 to 150 GPa for $MgSiO_3$ pv and from 100 to 150 GPa for $MgSiO_3$ ppv. Our results suggest that pressure increasingly suppresses defect population in the both phases because the defect formation enthalpies are shown to increase with increasing pressure. This means that defect formation at the lower mantle conditions should be predominantly extrinsic in the nature involving reactions between $MgSiO_3$ and coexisting (Mg,Fe)O, and impurities such as Fe, Al and protons. On the other hand, the predicted values of activation enthalpies and volumes of ionic diffusion differ largely between the two phases. In pv, Mg and Si are much slower moving ionic species, compared to O at all pressures. However, in ppv, the calculated activation enthalpies and volumes for Mg and Si are much smaller thereby making movement of all three species equally easy and much easier in ppv, compared to the corresponding cationic movements in pv. In the high-pressure regime near the bottom of the lower mantle where ppv is expected to be stable, extrinsic processes are expected to dominate defect formation and diffusion for all three species. Visualization of simulation data suggests that the charged point defects induce substantial distortions in the surrounding atomic and electronic structures. Both Mg and Si diffusion in ppv occur parallel to the *a*-axis. For instance, the Si migration path is contained in the SiO_6 layer, and it passes through the octahedral edges thereby pushing O atoms away from its path.

In this study, we have simulated the simplest cases of sublattice vacancies and ionic diffusion in $MgSiO_3$ pv and ppv. It is important to investigate more complex mechanisms such as coupled diffusion or diffusion in the presence of vacancies of other types. Such studies will involve consideration of a large number of possible defect configurations and also require a large supercell to accommodate more than a single defect. Previous (Wright and Price, 1993) and present simulations of Si diffusion in the presence of an O vacancy in pv predicted substantial changes in the values of activation enthalpy and volume. For instance, the activation enthalpy is reduced by O vacancy, more at higher pressures, and as a result, the calculated activation volume becomes negative. Also important is to simulate interstitial mechanism for ionic diffusion (Walker et al., 2003), and for instance, find out how the activation enthalpies and favorable paths compare between vacancy and interstitial mechanisms.

Our results are expected to have two important geophysical implications for the lower mantle: First, the

predicted high mobility of all three ionic (Mg, Si and O) species in the ppv phase suggests that this phase is likely to be more conductive than the pv phase. This is consistent with the experimentally observed high electrical conductivity at high pressure of $CaIrO_3$-type $Al2O_3$ — an analog of $MgSiO_3$ ppv (Weir et al., 1996). The possibility of high conductivity of ppv supports a highly conductive D″ layer model as suggested previously (Oganov and Ono, 2005; Ono et al., 2006). Such a model can explain the observed changes in Earth's rotation period in the terms of electromagnetic core-mantle coupling (Holme, 1998a,b). Second, our predictions for easy cationic migrations within the layers (along the ⟨100⟩ direction) and anionic migration between the layers (along the ⟨110⟩ direction) in ppv can be associated with deformation processes that are active at deep mantle conditions. The dominant slip system in $MgSiO_3$ pv is known experimentally (Karato et al., 1995; Cordier et al., 2004). Arguments based on the layered structure of the ppv phase are used to imply that the slip system of this phase is likely to be [100]/(010) (Murakami et al., 2004; Oganov and Ono, 2004; Tsuchiya et al., 2004a,b; Iitaka et al., 2004). This is also supported by recent deformation experiments performed on polycrystalline $CaIrO_3$ ppv — an analog of $MgSiO_3$ (Yamazaki et al., 2006). However, theoretical calculations (Oganov et al., 2005) have suggested the slip system of $[1^{-}10]$ /(110) for ppv. The lattice preferred orientation arising from the [100] /(010) and $[1^{-}10]$ /(110) slip systems give rise to strong V_{SH}/V_{SV} anisotropy of 2.9 and 4.1 %, respectively, which is consistent with the observed seismic anisotropy in the D″ layer (Iitaka et al., 2004; Oganov et al., 2005; Wookey et al., 2005; Yamazaki et al., 2006).

Acknowledgments

This work was supported by the NSF Career grant (EAR 0347204). Computing facilities were provided by CCT at Louisiana State University.

References

Alfe, D., Gillan, M.J., 2005. The Schottky defect formation energy in MgO calculated by diffusion Monte Carlo. Phys. Rev., B 71, 220101.

Baroni, S., Giannozzi, P., Testa, A., 1987. Green's function approach to linear response in solid. Phys. Rev. Lett. 58, 1861–1864.

Bhattarai, D., Karki, B.B., 2006. Visualization of atomistic simulation data for spatio-temporal information. Proc. 14th Int'l. Conf. Central Europe Comp. Graphics Vis. Comp. Vision. ISBN: 80-86943-03-8, pp. 17–24.

Braithwaite, J.S., Wright, K., Catlow, C.R.A., 2003. A theoretical study of the energetic and IR frequencies of hydroxyl defects in forsterite. J. Geophys. Res. 108, 2284–2292.

Brodholt, J.P., 1997. Ab initio calculations on point defects in forsterite (Mg_2SiO_4) and implications for diffusion and creep. Am. Mineral. 82, 1049–1053.

Brodholt, J.P., Refson, K., 2000. An ab initio study of hydrogen in fosterite and a possible mechanism for hydrolytic weakening. J. Geophys. Res. 105, 18977–18982.

Carrasco, J., Gomes, J.R.B., Illas, F., 2004. Theoretical study of bulk and surface oxygen and aluminum vacancies in α-Al_2O_3. Phys. Rev., B 69, 064116.

Carrasco, J., Illas, F., Lopez, N., Kotomin, E.A., Zhukovskii, Y.F., Evarestov, R.A., Mastrikov, Y.A., Piskunov, S., Maier, J., 2006. First-principles calculations of the atomic and electronic structure of F centers in the bulk and on the (001) surface of $SrTiO_3$. Phys. Rev., B 73, 064106.

Cordier, P., Ungar, T., Zsoldos, L., Tichy, G., 2004. Dislocation creep in $MgSiO_3$ perovskite at conditions of the Earth's uppermost lower mantle. Nature 428, 837–840.

De Vita, A., Gillan, M.J., Lin, J.S., Payne, M.C., Stich, I., Clarke, L.J., 1992. Defect energetic in MgO treated by first-principles methods. Phys. Rev., B 46, 12964–12973.Defects in oxide materials from first principles. Phys. Rev. Lett. 68, 3319–3322.

Dobson, D., 2003. Oxygen ionic conduction in $MgSiO_3$ perovskite. Phys. Earth Planet. Inter. 139, 55–64.

Giannozzi, P., de Gironcoli, S., Pavone, P., Baroni, S., 1991. Ab initio calculations of phonon dispersions in semiconductors. Phys. Rev., B 43, 7231–7242.

Hermance, J.F., 1995. Electrical conductivity models of the crust and mantle. Global Earth Physics — A Handbook of Physical Constants. AGU, pp. 190–205.

Hirose, K., 2006. Postperovskite phase transition and its geophysical implications. Rev. Geophys. 44 (Art No. RG3001).

Holme, R., 1998a. Electromagnetic core-mantle coupling, I. Explaining decadal changes in the length of day. Geophys. J. Int. 132, 167–180.

Holme, R., 1998b. Electromagnetic core-mantle coupling, II. Probing deep mantle conductance. In: Gurnis, M., Wysession, M.E., Knittle, E., Buffett, B.A. (Eds.), The Core-Mantle Boundary Region. AGU, pp. 139–151.

Holzapfel, C., Rubie, D.C., Frost, D.J., Langenhorst, F., 2005. Fe–Mg interdiffusion in (Mg,Fe)SiO_3 perovskite and lower mantle reequilibration. Science 309, 1707–1710.

Iitaka, T., Hirose, K., Kawamura, K., Murakami, M., 2004. The elasticity of the $MgSiO_3$ post-perovskite phase in the Earth's lowermost mantle. Nature 430, 442–445.

Karato, S., Zhang, S.Q., Wenk, H.R., 1995. Superplasticity in Earth's lower mantle — evidence from seismic anisotropy and rock physics. Science 270, 458–461.

Karki, B.B., Khanduja, G., 2006a. Point defects in MgO at high pressure. Am. Mineral. 91, 511–516.

Karki, B.B., Khanduja, G., 2006b. Computer simulation and visualization of vacancy defects in $MgSiO_3$ perovskite. Model. Sim. Mat. Sci. Eng. 14, 1041–1052.

Khanduja, G., Karki, B.B., 2006. A systematic approach to multiple datasets visualization of scalar volume data. Int. Conf. Comp. Graph. Theory App. 59–66.

Lento, J., Mozoz, J.L., Nieminen, R.M., 2002. Charged point defects in semiconductors and the supercell approximation. J. Phys. C 14, 2637–2645.

Leslie, M., Gillan, M.J., 1985. The energy and elastic dipole tensor of defects in ionic crystals calculated by the supercell method. J. Phys. C 18, 973–982.

Monkhorst, H.J., Pack, J.D., 1976. Special points for Brillouin-zone integrations. Phys. Rev., B 13, 5188–5192.

Murakami, M., Hirose, K., Kawamura, K., Sata, N., Ohishi, Y., 2004. Post-perovskite phase transition in $MgSiO_3$. Science 304, 855–858.

Oganov, A.R., Ono, S., 2004. Theoretical and experimental evidence for a post-perovskite phase of $MgSiO_3$ in Earth's layer. Nature 430, 445–448.

Oganov, A.R., Ono, S., 2005. The high-pressure phase of alumina and implications of Earth D″ layer. Proc. Natl. Acad. Sci. 102, 10828–10831.

Oganov, A.R., Martonak, R., Laio, A., Raiteri, P., Parrinello, M., 2005. Anisotropy of Earth's D″ layer and stacking faults in the $MgSiO_3$ post-perovskite phase. Nature 438, 1142–1143.

Ono, S., Oganov, A.R., 2005. In situ observations of phase transition between perovskite and $CaIrO_3$-type phase in $MgSiO_3$ and pyrolytic mantle composition. Earth Planet. Sci. Lett. 236, 914–932.

Ono, S., Oganov, A.R., Koyama, T., Shimizu, H., 2006. Stability and compressibility of the high-pressure phases of Al_2O_3 up to 200 GPa: implications for the electrical conductivity of the base of the lower mantle. Earth Planet. Sci. Lett. 246, 326–335.

Tsuchiya, T., Tsuchiya, J., Umemoto, K., Wentzcovitch, R.M., 2004a. Phase transition in $MgSiO_3$ perovskite in the earth's lower mantle. Earth Planet. Sci. Lett. 224, 241–248.

Tsuchiya, T., Tsuchiya, J., Umemoto, K., Wentzcovitch, R.M., 2004b. Elasticity of post perovskite $MgSiO_3$. Geophys. Res. Lett. 31, L14603.

Tsuchiya, J., Tsuchiya, T., Wentzcovitch, R.M., 2005. Vibrational and thermodynamic properties of $MgSiO_3$ postperovskite. J. Geophys. Res. 110 (Art No. B02204).

Wall, A., Price, G.D., 1989. In: Navrotsky, A., Weidner, D.J. (Eds.), Defects and diffusion in $MgSiO_3$ perovskite Proc. Perovskite Chapman Conf., vol. 45. American Geophysical Union, Washington, DC, pp. 45–53.

Walker, A.M., Wright, K., Slater, B., 2003. A computational study of oxygen diffusion in olivine. Phys. Chem. Miner. 30, 536–545.

Watson, G.W., Wall, A., Parker, S.C., 2000. Atomistic simulation of the effect of temperature and pressure on point defect formation in $MgSiO_3$ perovskite and the stability of $CaSiO_3$. J. Phys. C 12, 8427–8438.

Weir, S.T., Mitchell, A.C., Nellis, W.J., 1996. Electrical resistivity of single-crystal Al2O3 shock-compressed in the pressure range 91–220 GPa (0.91–2.20 Mbar). J. Appl. Phys. 80, 1522–1524.

Wentzcovitch, R.M., Tsuchiya, T., Tsuchiya, J., 2006. $MgSiO_3$ postperovskite at D″ conditions. Proc. Natl. Acad. Sci. 103, 543–546.

Wookey, J., Stackhouse, S., Kendall, M., Brodholt, J.P., Price, G.D., 2005. Efficacy of post-perovskite as an explanation for lowermost mantle seismic properties. Nature 438, 1004–1007.

Wright, K., Price, G.D., 1993. Computer simulations of defects and diffusion in perovskites. J. Geophys. Res. 98, 22245–22253.

Yamazaki, D., Kato, T., Yurimoto, H., Ohtani, E., Toriumi, M., 2000. Silicon self-diffusion in $MgSiO_3$ perovskite at 25 GPa. Phys. Earth Planet. Inter. 119, 299–309.

Yamazaki, D., Yoshino, T., Ohfuji, H., Ando, J.-i., Yoneda, A., 2006. Origin of seismic anisotropy in the D″ layer inferred from shear deformation experiments on post-perovskite phase. Earth Planet. Sci. Lett. 252, 372–378.

Van Orman, J.A., Fei, Y., Hauri, E.H., Wang, J., 2003. Diffusion in MgO at high pressures: Constraints on deformation mechanisms and chemical transport at the core–mantle boundary James. Geophys. Res. Lett. 30, 1056. doi:10.1029/2002GL016343.